

Modulation, ISI, and Detection for Langmuir Adsorption-Based Microfluidic Molecular Communication

Ruifeng Zheng, *Graduate Student Member, IEEE*, Pengjie Zhou, Pit Hofmann, *Graduate Student Member, IEEE*, Martín Schottlender, Fatima Rani, *Member, IEEE*, Juan A. Cabrera, and Frank H. P. Fitzek, *Fellow, IEEE*

Abstract—This paper studies microfluidic molecular communication receivers with finite-capacity Langmuir adsorption driven by an effective surface concentration. In the reaction-limited regime, we derive a closed-form single-pulse response kernel and a symbol-rate recursion for on-off keying that explicitly exposes channel memory and inter-symbol interference. We further develop short-pulse and long-pulse approximations, revealing an interference asymmetry in the long-pulse regime due to saturation. To account for stochasticity, we adopt a finite-receptor binomial counting model, employ pulse-end sampling, and propose a low-complexity midpoint-threshold detector that reduces to a fixed threshold when interference is negligible. Numerical results corroborate the proposed characterization and quantify detection performance versus pulse and symbol durations.

Index Terms—Molecular communication, Langmuir adsorption, microfluidics, biosensor receiver, binomial counting noise, threshold detection.

I. INTRODUCTION

MICROFLUIDIC molecular communication (MC) with surface-based biosensors is a promising paradigm for enabling reliable information transfer in lab-on-a-chip platforms and bio-nanotechnological systems, where information molecules (IMs) are transported by laminar flow and detected via reversible binding to receptors on a sensing surface [2]–[4]. Such receivers are attractive for applications including in situ biochemical sensing, closed-loop synthetic biology, and microfluidic diagnostics, as they can directly interface chemical signals with electronic readout circuits (e.g., field-effect transistor biosensors) [5]–[7]. A central challenge, however,

A preliminary version of the receiver model appears in [1].

R. Zheng, P. Zhou, P. Hofmann, M. Schottlender, F. Rani, J. A. Cabrera, and F. H. P. Fitzek are with the Deutsche Telekom Chair of Communication Networks, Dresden University of Technology, Germany; P. Hofmann, J. Cabrera, and F. Fitzek are also with the Centre for Tactile Internet with Human-in-the-Loop (CeTI), Dresden, Germany, email: {ruifeng.zheng, pengjie.zhou, pit.hofmann, martin.schottlender, fatima.rani, juan.cabrera, frank.fitzek}@tu-dresden.de.

This work was funded by the German Research Foundation (DFG, Deutsche Forschungsgemeinschaft) as part of Germany's Excellence Strategy – EXC 2050/2 – Project ID 390696704 – Cluster of Excellence “Centre for Tactile Internet with Human-in-the-Loop” (CeTI) of Dresden University of Technology. The authors also acknowledge the financial support by the Federal Ministry of Research, Technology and Space (BMFTR) of Germany in the program “Souverän. Digital. Vernetzt.” Joint project 6G-life, project identification number 16KIS2413K, and the program “Verbundprojekt: Disruptive Kommunikationsparadigmen für technologische Souveränität, Resilienz und Shared Prosperity - Translation in Industrie und Aufbau innovativer Technologiedemonstratoren - CommUnity,” project identification number 16KISS012K. Furthermore, this work was partly supported by the projects IoBNT (grant number 16KIS1994) and MoMiKoSy (Software Campus, grant number 16S23070), funded by the Federal Ministry of Research, Technology and Space (BMFTR).

lies in accurately characterizing the *receiver dynamics* under realistic biochemical constraints. In particular, finite receptor capacity and reversible binding/unbinding kinetics introduce nonlinear saturation and a persistent temporal memory [1], [3], [4], which shape inter-symbol interference (ISI) and fundamentally impact detection performance [1], [5], [8], [9].

Many MC studies model the receiver as an instantaneous detector once IMs reach the sensing surface [8], [10]–[12]. In contrast, practical surface-based biosensors often operate in a *reaction-limited* regime, where binding/unbinding kinetics dominate the sensing timescale and introduce latency and temporal memory [3]. Existing receiver models span passive concentration sensing and active boundary interactions (e.g., absorption or reversible adsorption) [8], [10], [13], [14]. For microfluidic biosensing, a convection–diffusion–reaction framework with finite reactive surfaces was developed in [5], and graphene field-effect transistor (GFET)-based DNA biosensor receivers were experimentally demonstrated in [6]. Despite these advances, a communication-oriented *symbol-level* characterization that reveals how finite-receptor Langmuir dynamics induce ISI under on-off keying (OOK) and enables low-complexity detection and error-performance evaluation under counting noise remains needed.

Motivated by this need, we consider OOK signaling in which mass transport is abstracted into a time-varying *effective surface concentration* driving Langmuir adsorption at the receiver surface. The finite-receptor reaction dynamics govern how quickly the receiver output rises during molecule injection and decays after injection stops, yielding distinct short-pulse (SP) and long-pulse (LP) behaviors. A preliminary receiver modeling study appears in [1]. Here, we substantially extend it to an end-to-end symbol-rate communication framework by incorporating modulation, ISI analysis, and detection. This work is also complementary to our Markov-based framework for DNA-based MC [15], focusing on adsorption-based biosensor receivers and their implications for symbol-level performance.

The main contributions of this paper are summarized as follows: (1) We model microfluidic transport via an effective surface concentration driving finite-capacity Langmuir adsorption and derive a symbol-rate recursion that exposes channel memory and ISI; (2) we derive a closed-form single-pulse response kernel and develop short-/long-pulse (SP/LP) approximations for characterizing the symbol-rate response and ISI; and (3) we incorporate finite-receptor binomial counting noise, adopt pulse-end sampling, and propose a low-complexity midpoint-threshold detector for performance evaluation.

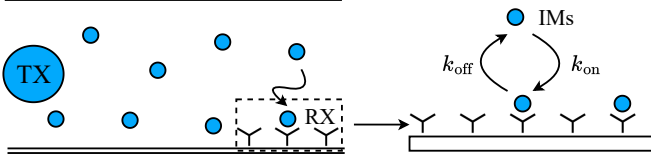


Fig. 1. Schematic illustration of reversible binding of IMs at the receiver surface.

II. SYSTEM MODEL

In this section, we describe the considered microfluidic MC system with a surface-based biosensor receiver, including the transport-driven effective surface concentration model, the OOK modulation scheme, and the resulting Langmuir adsorption dynamics. We then derive the single-pulse response kernel and use it to characterize the deterministic response to an OOK symbol sequence, highlighting the origin of ISI and providing SP and LP approximations that will be used later for performance analysis.

A. System Overview

We consider a microfluidic conduit that releases IMs from the transmitter to a surface-based biosensor receiver with N_p identical, non-interacting binding sites, see Fig. 1. Under stable laminar flow and diffusion-assisted mixing, the transport effects near the sensing surface are captured by a time-varying *effective surface concentration* $c(t)$, consistent with [2], [3]. In this paper, we treat $c(t)$ as the effective channel input; the mapping from the injected waveform to $c(t)$ can be obtained from a transport model and is established in our prior work [1].

Under the *reaction-limited* assumption, the mean number of occupied sites $N_b(t) \in [0, N_p]$ evolves according to the Langmuir kinetics

$$\frac{dN_b(t)}{dt} = k_{\text{on}}c(t)(N_p - N_b(t)) - k_{\text{off}}N_b(t), \quad (1)$$

where k_{on} and k_{off} are the binding and unbinding rate constants, respectively.

B. Transmitter Modulation

We consider OOK modulation with a symbol interval T_b and pulse duration $T \leq T_b$. The symbol 1 is represented by a rectangular concentration pulse of amplitude c_0 and duration T , while the symbol 0 corresponds to no pulse. For a symbol sequence $\{a_i\}_{i=0}^{K-1}$, $a_i \in \{0, 1\}$, let $t_i \triangleq iT_b$ denote the start time of the i -th symbol. The resulting effective surface concentration is

$$x(t) \triangleq c(t) = c_0 \sum_{i=0}^{K-1} a_i [u(t - t_i) - u(t - t_i - T)], \quad (2)$$

where $u(t)$ is the unit-step function. For a single bit-1 pulse starting at $t_0 = 0$, Eq. (2) reduces to $x(t) = c_0[u(t) - u(t - T)]$.

C. Single-Pulse Response Kernel

We define the *single-pulse response kernel* $h_T(t)$ as the zero-state response (i.e., $N_b(0) = 0$) to a single rectangular pulse in Eq. (2). Solving Eq. (1) yields

$$h_T(t) = \begin{cases} 0, & t \leq 0, \\ N_b^\infty [1 - \exp(-t/\tau_{\text{on}})], & 0 < t \leq T, \\ N_b^\infty \exp[-(t - T)/\tau_{\text{off}}], & t > T, \end{cases} \quad (3)$$

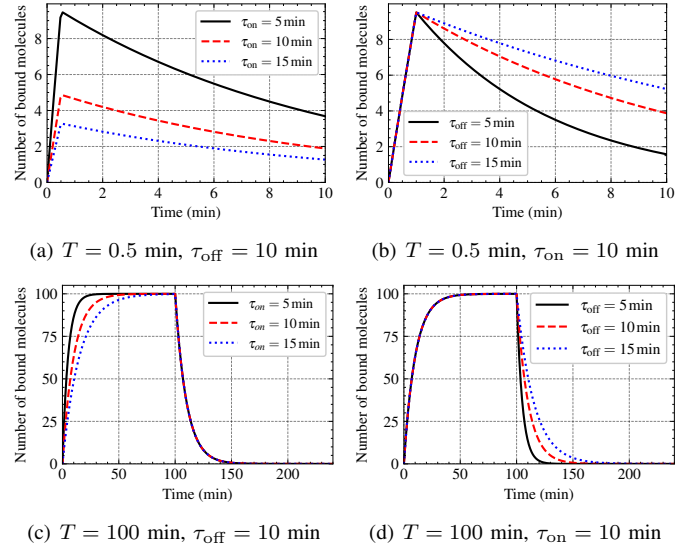


Fig. 2. Single-pulse response kernel $h_T(t)$ in the SP and LP regimes, illustrating the impact of τ_{on} on the rise phase and τ_{off} on the post-pulse decay (temporal memory).

where the steady bound count and the characteristic binding/unbinding time constants are

$$N_b^\infty = N_p \frac{c_0/K_D}{1 + c_0/K_D}, \quad \tau_{\text{on}} = \frac{1}{k_{\text{on}}c_0 + k_{\text{off}}}, \quad \tau_{\text{off}} = \frac{1}{k_{\text{off}}}, \quad (4)$$

with dissociation constant $K_D = k_{\text{off}}/k_{\text{on}}$. Moreover, the bound count at the end of the concentration pulse is

$$N_b^{\text{end}} \triangleq h_T(T) = N_b^\infty [1 - \exp(-T/\tau_{\text{on}})], \quad (5)$$

which is the pulse-end (and peak) value of $h_T(t)$. The time constants τ_{on} and τ_{off} characterize the rise and decay dynamics of the receiver response, respectively; in particular, τ_{off} governs the post-pulse decay and thus the effective temporal memory. This temporal memory implies that residual bound molecules remain after the pulse ends and interfere with subsequent symbols, thereby giving rise to ISI.

In the SP regime, we approximate the exponential rise by its first-order expansion. Specifically, for $T \leq 0.2 \tau_{\text{on}}$, the kernel in Eq. (3) can be approximated as

$$h_{\text{SP}}(t) \approx \begin{cases} 0, & t \leq 0, \\ N_b^\infty \frac{t}{\tau_{\text{on}}}, & 0 < t \leq T, \\ N_b^\infty \frac{T}{\tau_{\text{on}}} \exp[-(t - T)/\tau_{\text{off}}], & t > T. \end{cases} \quad (6)$$

In the LP regime, the response approaches the steady-state within the pulse. In particular, for $T \geq 5 \tau_{\text{on}}$ we have $\exp(-T/\tau_{\text{on}}) \leq e^{-5}$ and thus $N_b^{\text{end}} \approx N_b^\infty$; the initial rise transient of duration is negligible relative to the pulse duration. Therefore, we adopt the LP approximation

$$h_{\text{LP}}(t) \approx \begin{cases} 0, & t \leq 0, \\ N_b^\infty, & 0 < t \leq T, \\ N_b^\infty \exp[-(t - T)/\tau_{\text{off}}], & t > T. \end{cases} \quad (7)$$

Fig. 2 illustrates $h_T(t)$ in the SP and LP regimes. In Figs. 2(a) and 2(c), varying τ_{on} mainly changes the rise behavior within the pulse, whereas in Figs. 2(b) and 2(d), varying τ_{off} directly controls the post-pulse decay tail. A larger τ_{off} yields a slower decay and a longer *temporal memory*, meaning that the response to a symbol persists into subsequent symbol intervals and becomes the primary physical source of ISI in this work.

D. Deterministic Response of OOK Sequence

We characterize the deterministic (mean) binding response $y(t) \triangleq N_b(t)$ to an OOK symbol sequence driven by the effective surface concentration $c(t)$ in Eq. (2). Let $t_i \triangleq iT_b$ for $i = 0, 1, \dots, K-1$, define the symbol-start state $Y_i \triangleq y(t_i)$, and denote the pulse-end sampling time by

$$t_{s,i} \triangleq t_i + T. \quad (8)$$

Substituting Eq. (2) into Eq. (1), the exact response within the i -th symbol interval $t \in [t_i, t_{i+1})$ (where $t_{i+1} = t_i + T_b$) is given as follows.

For $a_i = 1$,

$$y(t) = \begin{cases} N_b^\infty + (Y_i - N_b^\infty) \exp\left(-\frac{t - t_i}{\tau_{\text{on}}}\right), & t \in [t_i, t_{s,i}), \\ y(t_{s,i}) \exp\left(-\frac{t - t_{s,i}}{\tau_{\text{off}}}\right), & t \in [t_{s,i}, t_{i+1}), \end{cases} \quad (9)$$

where the pulse-end response is

$$y(t_{s,i}) = N_b^\infty + (Y_i - N_b^\infty) \exp(-T/\tau_{\text{on}}). \quad (10)$$

For $a_i = 0$,

$$y(t) = Y_i \exp(-(t - t_i)/\tau_{\text{off}}), \quad t \in [t_i, t_{i+1}). \quad (11)$$

Evaluating at $t = t_{i+1}$ yields the closed-form recursion

$$Y_{i+1} = \begin{cases} y(t_{s,i}) \exp(-(T_b - T)/\tau_{\text{off}}), & a_i = 1, \\ Y_i \exp(-T_b/\tau_{\text{off}}), & a_i = 0, \end{cases} \quad (12)$$

which explicitly reveals how past symbols determine the evolution of the symbol-start state sequence $\{Y_i\}$.

E. Kernel-Based SP/LP Approximations

In the SP regime, we employ the SP kernel approximation in Eq. (6). When the occupancy remains low (so that the Langmuir dynamics can be well approximated by a linearization around the operating point), the overall response can be approximated by a superposition of shifted single-pulse kernels, i.e.,

$$y_{\text{SP}}(t) \approx \sum_{i=0}^{K-1} a_i h_{\text{SP}}(t - iT_b), \quad (13)$$

where $h_{\text{SP}}(t)$ is given in Eq. (6).

In the LP regime, the binding response approaches steady state within the pulse; for $T \geq 5\tau_{\text{on}}$ we have $N_b^{\text{end}} \approx N_b^\infty$ and thus the LP kernel approximation in Eq. (7) applies. Since saturation makes the system generally not linear time-invariant (LTI), the following expression should be understood as a pulse-wise benchmark approximation. When ISI is negligible (e.g., sufficiently large T_b), we use

$$y_{\text{LP}}(t) \approx \sum_{i=0}^{K-1} a_i h_{\text{LP}}(t - iT_b), \quad (14)$$

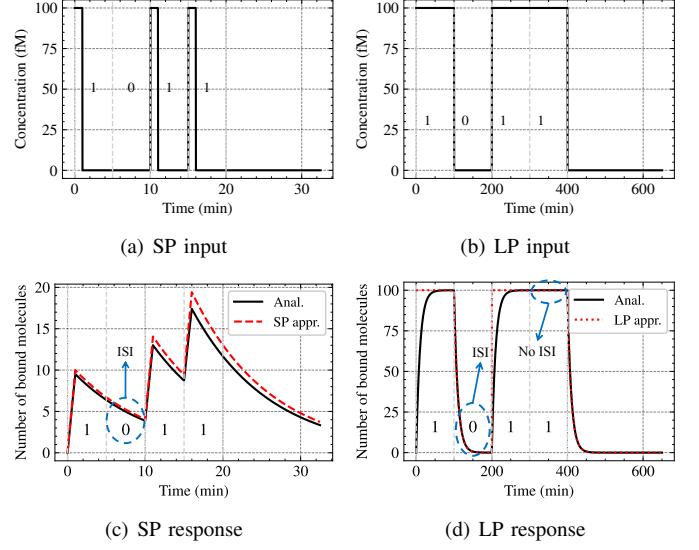


Fig. 3. Illustration of OOK modulation and deterministic receiver response for the symbol sequence $[1, 0, 1, 1]$ in the SP ($T = 0.1\tau_{\text{on}}$, $T_b = 0.5\tau_{\text{on}}$) and LP ($T = 10\tau_{\text{on}}$, $T_b = 10\tau_{\text{on}}$) regimes. (a),(c) correspond to SP signaling and compare the analytical response with the SP approximation; (b),(d) correspond to LP signaling and compare the analytical response with the LP approximation. Parameters: $\tau_{\text{on}} = 10$ min and $\tau_{\text{off}} = 10$ min.

TABLE I
SIMULATION PARAMETERS.

Parameter	Symbol	Value	Unit
Number of transmitted symbols	K	10^5	–
Number of binding sites	N_p	10^6	–
Binding rate constant	k_{on}	10^8	$\text{M}^{-1}\text{min}^{-1}$
Unbinding rate constant	k_{off}	0.1	min^{-1}
Pulse concentration	c_0	100	fM

where $h_{\text{LP}}(t)$ is given in Eq. (7).

F. ISI Mechanism and Asymmetry

Fig. 3 compares SP and LP signaling for the same symbol sequence. In the SP case (Fig. 3(c)), the receiver operates in a low-occupancy regime, where the adsorption dynamics are approximately linear, and the response resembles that of classical passive-receiver models: ISI is primarily induced by the exponential dissociation (unbinding) tail of previously bound molecules, governed by τ_{off} . In the LP case (Fig. 3(d)), receptor saturation introduces a pronounced asymmetry. For $1 \rightarrow 0$ transitions, residual bound molecules after pulse end yield appreciable ISI. In contrast, for $1 \rightarrow 1$ transitions, the bound count is already close to saturation (limited by the finite binding-site capacity N_p), so the additional ISI contribution is small and the resulting ISI is substantially reduced. This asymmetry will be reflected in the detection and error-performance results in later sections.

III. NOISY OBSERVATION MODEL AND DETECTION

In this section, we incorporate receiver noise and develop a low-complexity detection scheme. Specifically, we model the observed bound count using a finite-receptor binomial counting model, define a pulse-end sampling statistic, and apply a simple midpoint-threshold detector. For the special

case of negligible ISI, the detector further reduces to a fixed threshold.

A. Noisy Observation Model

The receiver output $y(t) \triangleq N_b(t)$ in Eqs. (9) and (11) represents the deterministic (mean) number of occupied binding sites. Since binding and unbinding are stochastic events over a finite population of N_p sites, we model the measured bound count as a binomial random variable. Let $\tilde{N}_b(t)$ denote the observed number of occupied sites at time t . Conditioned on the mean occupancy probability $p(t) \triangleq y(t)/N_p$, we assume

$$\tilde{N}_b(t) \mid y(t) \sim \mathcal{B}(N_p, p(t)), \quad (15)$$

where $\mathcal{B}(n, p)$ denotes a binomial distribution with n independent trials and success probability p .

For analytical tractability, we also employ a Poisson approximation. When N_p is large and $p(t)$ is small such that $N_p p(t) = y(t)$ remains finite, the conditional distribution in Eq. (15) can be approximated as

$$\tilde{N}_b(t) \mid y(t) \approx \mathcal{P}(y(t)), \quad (16)$$

where $\mathcal{P}(\lambda)$ denotes a Poisson distribution with mean λ .

B. Sampling and Decision Statistic

We sample the receiver output at the pulse-end time $t_{s,i}$ defined in Eq. (8), and define the decision statistic

$$z_i \triangleq \tilde{N}_b(t_{s,i}). \quad (17)$$

Let $\mu_{m,i} \triangleq \mathbb{E}\{z_i \mid \mathcal{H}_m\}$ denote the conditional mean under hypothesis \mathcal{H}_m ($m \in \{0, 1\}$, corresponding to $a_i = m$). From Eqs. (9) and (11), we obtain

$$\mu_{1,i} = y(t_{s,i}) = N_b^\infty + (Y_i - N_b^\infty) \exp(-T/\tau_{\text{on}}), \quad (18)$$

$$\mu_{0,i} = y(t_{s,i}) = Y_i \exp(-T/\tau_{\text{off}}), \quad (19)$$

where $Y_i \triangleq y(t_i)$ is the symbol-start state. Accordingly, under the binomial counting model in Eq. (15),

$$z_i \mid \mathcal{H}_m \sim \mathcal{B}(N_p, \mu_{m,i}/N_p), \quad m \in \{0, 1\}. \quad (20)$$

C. Midpoint-Threshold Detector

To keep the detection rule simple, we adopt an integer-valued midpoint threshold

$$\eta_i \triangleq \left\lfloor \frac{\mu_{0,i} + \mu_{1,i}}{2} \right\rfloor, \quad (21)$$

and decide

$$\hat{a}_i = \begin{cases} 1, & z_i > \eta_i, \\ 0, & z_i \leq \eta_i, \end{cases} \quad (22)$$

where $\lfloor \cdot \rfloor$ denotes rounding to the nearest integer.

Since η_i depends on the symbol-start state Y_i , we employ a decision-feedback (DF) state tracker [16]. Specifically, the receiver maintains a symbol-rate state estimate \hat{Y}_i , initializes $\hat{Y}_0 = 0$, and computes η_i by substituting \hat{Y}_i into Eqs. (18) and (19). After deciding \hat{a}_i using Eq. (22), the state estimate is updated via the same recursion as Eq. (12) with a_i replaced by \hat{a}_i , i.e.,

$$\hat{Y}_{i+1} = \begin{cases} \mu_1(\hat{Y}_i) \exp[-(T_b - T)/\tau_{\text{off}}], & \hat{a}_i = 1, \\ \hat{Y}_i \exp(-T_b/\tau_{\text{off}}), & \hat{a}_i = 0, \end{cases} \quad (23)$$

where $\mu_1(\hat{Y}_i) \triangleq N_b^\infty + (\hat{Y}_i - N_b^\infty) \exp(-T/\tau_{\text{on}})$.

When ISI is negligible (e.g., T_b is large enough that the residual occupancy decays to $Y_i \approx 0$ at the beginning of symbol i), the conditional means satisfy $\mu_{0,i} \approx 0$ and $\mu_{1,i} \approx N_b^{\text{end}}$; hence, a fixed midpoint threshold $\eta \approx \lfloor N_b^{\text{end}}/2 \rfloor$ is sufficient.

IV. NUMERICAL RESULTS

In this section, we present numerical evaluations to quantify the bit error ratio (BER) performance of the proposed pulse-end sampling and DF midpoint-threshold detector under binomial counting noise. All simulations are conducted in MATLAB, with the parameters summarized in Table I, unless otherwise specified.

A. Simulation Setup

We consider OOK modulation with pulse duration T and symbol interval T_b . For each configuration, we generate K independent and identically distributed (i.i.d.) equiprobable symbols and compute the mean state evolution via the recursion in Eq. (12). Noisy pulse-end samples $z_i = \tilde{N}_b(t_{s,i})$ with $t_{s,i} = t_i + T$ are drawn from the binomial counting model in Eq. (15), and symbols are detected using Eq. (21) with DF state tracking based on Eq. (12). The BER is estimated as

$$\text{BER} \triangleq \frac{1}{K} \sum_{i=0}^{K-1} \mathbb{1}\{\hat{a}_i \neq a_i\}, \quad (24)$$

where $\mathbb{1}\{\cdot\}$ denotes the indicator function, i.e., $\mathbb{1}\{A\} = 1$ if A is true and $\mathbb{1}\{A\} = 0$ otherwise.

B. Impact of Symbol Interval

In the considered Langmuir adsorption-based microfluidic MC system, the dominant performance limitation is ISI induced by the receptor temporal memory. Increasing the symbol interval T_b allows the bound count to relax further between symbols, thereby mitigating ISI. Fig. 4(a) shows the BER as a function of the symbol interval T_b for several pulse durations T , with the constraint $T \leq T_b$. As T_b increases from 3 min to 50 min, all BER curves decrease monotonically. This behavior confirms that T_b is the main design parameter controlling ISI, since a larger T_b provides more time for the post-pulse dissociation to reduce the residual occupancy before the next symbol starts.

Moreover, the BER reduction becomes marginal once T_b exceeds approximately 30 min. This saturation is consistent with the temporal-memory decay governed by τ_{off} (here $\tau_{\text{off}} = 10$ min). After the pulse ends, the residual response decays exponentially as $\exp(-\Delta/\tau_{\text{off}})$, thus, at $\Delta = \tau_{\text{off}}$ it drops to $e^{-1} \approx 37\%$ of its pulse end value, at $\Delta = 3\tau_{\text{off}}$ to $e^{-3} \approx 5\%$, and at $\Delta = 5\tau_{\text{off}}$ to $e^{-5} \approx 0.7\%$ (see details in [1]). Therefore, when $T_b \gtrsim 3\tau_{\text{off}}$, the residual occupancy carried into the next symbol is already small, and further increasing T_b yields only limited additional ISI mitigation, resulting in an approximately flat BER.

For a fixed symbol interval T_b , the BER decreases as the pulse duration T increases. A longer pulse yields a larger pulse-end bound count N_b^{end} (cf. Eq. (5)), thereby increasing the sampled mean under \mathcal{H}_1 (i.e., $\mu_{1,i}$ in Eq. (18)). Consequently, the mean separation between the two hypotheses at

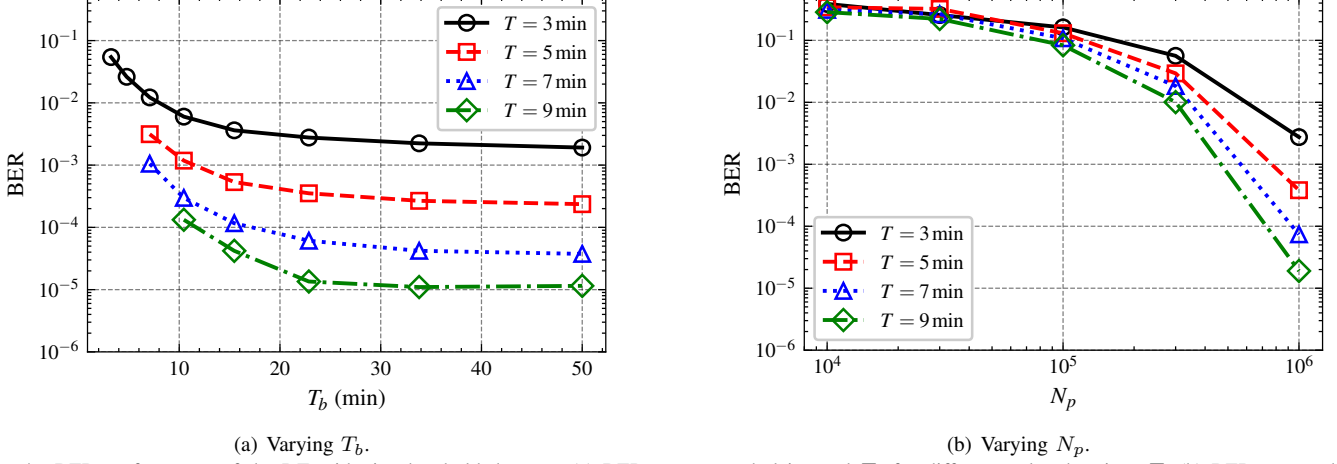


Fig. 4. BER performance of the DF midpoint-threshold detector. (a) BER versus symbol interval T_b for different pulse durations T . (b) BER versus the number of binding sites N_p for different T , with $T_b = 20$ min.

the sampling time increases, i.e., $\mu_{1,i} - \mu_{0,i}$ (cf. Eqs. (18) and (19)), which improves detectability. Under the binomial counting model, a larger mean count yields a more reliable pulse-end sample, resulting in a lower BER.

C. Impact of the Number of Binding Sites

Fig. 4(b) shows the BER as a function of the number of binding sites N_p for different pulse durations T . The symbol interval is fixed to $T_b = 20$ min, which corresponds to $2\tau_{\text{off}}$ for the considered parameters; thus, the residual response between adjacent symbols is noticeably reduced, and the performance trend is largely dominated by counting noise. As N_p increases from 10^4 to 10^6 , the BER decreases for all T . This is expected since the steady state bound count scales linearly with the number of available sites, i.e., $N_b^\infty \propto N_p$ in Eq. (4). With a small N_p (e.g., 10^4 – 10^5), the pulse-end mean bound count remains low, hence the binomial counting fluctuations are large relative to the mean, leading to unreliable decisions and an unacceptably high BER. As N_p grows (e.g., 10^5 – 10^6), the mean count increases while the relative counting uncertainty decreases, resulting in a higher effective SNR of the pulse-end statistic and a substantially lower BER.

For a fixed N_p , a larger T further improves performance. A longer pulse yields a larger pulse-end bound count N_b^{end} (cf. Eq. (5)), which increases the sampled mean under \mathcal{H}_1 and enlarges the mean separation between hypotheses (cf. Eqs. (18) and (19)). Consequently, the impact of counting noise becomes less pronounced, and the BER decreases.

V. CONCLUSION

This paper studied Langmuir adsorption-based microfluidic molecular communication with finite receptor capacity. We derived a closed-form single-pulse response kernel and a symbol-rate recursion for OOK, which together reveal the channel memory and the resulting ISI. We further developed SP/LP approximations and showed an LP ISI asymmetry induced by receptor saturation. To account for stochasticity, we adopted a binomial counting model and proposed a low-complexity pulse-end-sampling midpoint-threshold detector with decision-feedback (DF) state tracking. Numerical results validated the analysis and highlighted the impacts of T_b and N_p on ISI

and detection reliability. Future work includes joint transport-reaction modeling and optimized detection in the strong-ISI regime.

REFERENCES

- [1] R. Zheng *et al.*, “Molecular communication with Langmuir adsorption kinetics: Channel characteristics and temporal memory,” *IEEE Commun. Lett.*, vol. 30, pp. 787–791, Jan. 2026.
- [2] A. Hassibi *et al.*, “Real-time DNA microarray analysis,” *Nucleic Acids Res.*, vol. 37, no. 20, Aug. 2009, Art. no. e132.
- [3] T. M. Squires, R. J. Messinger, and S. R. Manalis, “Making it stick: Convection, reaction and diffusion in surface-based biosensors,” *Nat. Biotechnol.*, vol. 26, no. 4, pp. 417–426, Apr. 2008.
- [4] S. Xu *et al.*, “Real-time reliable determination of binding kinetics of DNA hybridization using a multi-channel graphene biosensor,” *Nat. Commun.*, vol. 8, no. 1, Mar. 2017, Art. no. 14902.
- [5] M. Kuscu and O. B. Akan, “Modeling convection-diffusion-reaction systems for microfluidic molecular communications with surface-based receivers in Internet of Bio-Nano Things,” *PloS One*, vol. 13, no. 2, Feb. 2018, Art. no. e0192202.
- [6] M. Kuscu *et al.*, “Fabrication and microfluidic analysis of graphene-based molecular communication receiver for Internet of Nano Things (IoNT),” *Sci. Rep.*, vol. 11, no. 1, Oct. 2021, Art. no. 19600.
- [7] M. Scherer *et al.*, “Closed-loop long-term experimental molecular communication system,” *IEEE Trans. Mol. Biol. Multi-Scale Commun.*, vol. 12, pp. 22–41, 2026.
- [8] Y. Deng *et al.*, “Modeling and simulation of molecular communication systems with a reversible adsorption receiver,” *IEEE Trans. Mol. Biol. Multi-Scale Commun.*, vol. 1, no. 4, pp. 347–362, Jul. 2015.
- [9] R. Zheng *et al.*, “ANIS: Anti-noise ISI-suppression filter for molecular communication via diffusion,” *IEEE Trans. Mol. Biol. Multi-Scale Commun.*, vol. 11, no. 4, pp. 572–587, Jun. 2025.
- [10] H. B. Yilmaz *et al.*, “Three-dimensional channel characteristics for molecular communications with an absorbing receiver,” *IEEE Commun. Lett.*, vol. 18, no. 6, pp. 929–932, Apr. 2014.
- [11] Y. Huang *et al.*, “Spatial modulation for molecular communication,” *IEEE Trans. Nanobiosci.*, vol. 18, no. 3, pp. 381–395, Mar. 2019.
- [12] R. Zheng, L. Lin, and H. Yan, “A noise suppression filter for molecular communication via diffusion,” *IEEE Wirel. Commun. Lett.*, vol. 10, no. 3, pp. 589–593, Nov. 2020.
- [13] N. Farsad *et al.*, “A comprehensive survey of recent advancements in molecular communication,” *IEEE Commun. Surveys Tuts.*, vol. 18, no. 3, pp. 1887–1919, Feb. 2016.
- [14] W. Guo *et al.*, “Molecular communications: Channel model and physical layer techniques,” *IEEE Wirel. Commun.*, vol. 23, no. 4, pp. 120–127, Aug. 2016.
- [15] R. Zheng *et al.*, “DNA-based molecular communication: A Markov approach to channel modeling and detection,” in *Proc. IEEE Globecom*, Dec. 2025, accepted for publication.
- [16] C. A. Belfiore and J. H. Park, “Decision feedback equalization,” *Proc. IEEE*, vol. 67, no. 8, pp. 1143–1156, Aug. 1979.